Draft, February 5, 2008
Preprint typeset using LaTeX style emulateapj v. 02/07/07

arXiv:0705.3649v2 [astro-ph] 17 Jun 2007

ON THE ORIGIN OF KINEMATIC DISTRIBUTION OF THE SUB-PARSEC YOUNG STARS IN THE GALACTIC CENTER

Qingjuan Yu[1,3], Youjun Lu[1], & D. N. C. Lin[1,2]
[1]Department of Astronomy and Astrophysics, University of California, Santa Cruz, CA 95064, USA
[2]Kavli Institute of Astronomy & Astrophysics, Peking University, Beijing, China
Draft, February 5, 2008

ABSTRACT

Observations indicate the presence of a massive black hole in the Galactic center. Within a half-parsec from the Galactic center, there is a population of coeval young stars which appear to reside in a coherent disk. Surrounding this dynamically-cool stellar system, there is a population of stars with a similar age and much larger eccentricities and inclinations relative to the disk. We propose a hypothesis for the origin of this dynamical dichotomy. Without specifying any specific mechanism, we consider the possibility that both stellar populations were formed within a disk some 6±2 Myr ago. But this orderly structure was dynamically perturbed outside-in by an intruding object with a mass $\sim 10^4 M_\odot$, which may be an intermediate-mass black hole or a dark stellar cluster hosting an intermediate-mass black hole. We suggest that the perturber migrated inward to $\sim 0.15 - 0.3\,\mathrm{pc}$ from the Galactic center as a consequence of orbital decay under the action of dynamical friction. Along the way, it captured many stars in the outer disk region into its mean-motion resonance, forced them to migrate with it, closely encountered with them, and induced the growth of their eccentricity and inclination. But stars in the inner regions of the disk retain their initial coplanar structure. Quantitatively, a perturber on a low-inclination or overhead orbit to the disk plane can reproduce the observed kinematic structure of these young stars. But this process is unlikely to produce the controversial two-disk structure. We predict that some of the inclined and eccentric stars surrounding the disk may have similar Galactocentric semimajor axis. Future precision determination of their kinematic distribution of these stars will not only provide a test for this hypothesis but also evidences for the presence of an intermediate-mass black hole or a dark cluster at the immediate proximity of the massive black hole at the Galactic center.
Subject headings: Black hole physics: Galaxy: center-stars: kinematics and dynamics: stellar dynamics

1. INTRODUCTION

Recent observations show that a large number of early-type stars, either O/W-R stars or less massive B stars (totally about 90), reside within the central half-parsec region of the Galactic center (GC) (Genzel et al. 2003; Ghez et al. 2003, 2005; Paumard et al. 2006, and references therein). These young stars have some distinctive features (Levin & Beloborodov 2003; Genzel et al. 2003; Paumard et al. 2006): (a) About 26 stars are found to reside in a well-defined and moderately thin disk, which rotates clockwise in projection and has a scale height-to-radius ratio $h/r \sim 0.12 \pm 0.03$. According to Paumard et al. (2006), about a dozen stars reside in a less well-defined counterclockwise rotating disk and these two disks are orientated at a large angle ($\sim 110^\circ$) with each other. Note that the existence of the counterclockwise rotating disk is still in controversy; nevertheless, observations indicate that the motion of some stars (probably located at the outer region, see item c below) is non-coplanar with respect to that of stars in the clockwise rotating disk. (b) The stars in the clockwise rotating disk are on low-eccentricity orbits (with eccentricity $e \sim 0.2 - 0.4$ on average). In contrast, many stars in the counterclockwise disk appear to be on high-eccentricity orbits (say, $e \sim 0.8$). (c) The clockwise rotating disk is compact and has a sharp inner edge at $\sim 1''$ ($\sim 0.04\,\mathrm{pc}$ with an assumed GC's heliocentric distance of 8 kpc), while the counterclockwise component has a ring-like structure which is located further out at $\sim 4''$ ($\sim 0.15\,\mathrm{pc}$). (d) The stars in the "two disks" are coeval with an age of $6 \pm 2\,\mathrm{Myr}$ and probably formed within a time span of $\lesssim 2\,\mathrm{Myr}$. (e) A cluster of main-sequence B stars ($4\,\mathrm{M}_\odot \leq M_* \leq 15\,\mathrm{M}_\odot$) or the so-called "S-cluster" exists in the inner $\sim 0.04\,\mathrm{pc}$ region, which has a spatially isotropic distribution and is distinct from the more massive sub-parsec ($\sim 0.04 - 0.5\,\mathrm{pc}$) young stars. Some of these S-stars have high eccentricities (with e up to 0.9–1) while others have moderate eccentricities. The S-star orbits have provided strong evidence for the existence of a massive black hole (MBH; with mass $M_{\rm BH} \simeq 3.6 \times 10^6\,\mathrm{M}_\odot$) in the GC (Schödel et al. 2002; Ghez et al. 2005; Eisenhauer et al. 2005, and references therein). The young stars in the GC, together with the central MBH, provide an interesting dynamical system to study. Specifically, the dynamical architecture of the GC resembles that of the solar system, which is composed of a thin disk of major planets and a thick population of minor planets orbiting around the Sun. As studies of the dynamics in our solar system have provided us considerable insights on the formation and evolution of the Sun and its surrounding planets, investigations on the dynamical system in the GC may also provide us insights into the structure, and the formation and evolution of the central MBH and stars in the nucleus of our own Galaxy and further in general galactic nuclei.

Electronic address: yqj, lyj, lin@ucolick.org
[3] Also a Hubble Fellow at the Department of Astronomy, University of California at Berkeley, Berkeley, CA 94720.

The coevality of the sub-parsec young stars suggests that they have a common origin. Since the tidal force of the central MBH may prevent formation of young stars through the collapse of self-gravitating cold molecular gas clouds in the vicinity of the MBH (e.g., Sanders 1992; Morris 1993), other hypothesis have been proposed to explain the formation and youth of the stars, including some non-conventional *in situ* formation scenario and in-spiraling young star cluster scenario. The *in situ* formation scenario is based on the assumption that the young stars were formed via the onset of gravitational instability and fragmentation in a hypothetical accretion disk around the MBH which no longer exist today. With a sufficiently large gas surface density, the self-gravity of the perturbation may overcome the impediment of the MBH's tidal force (e.g., Levin & Beloborodov 2003; Genzel et al. 2003; Goodman 2003; Levin 2007). In the in-spiraling star cluster scenario, it is assumed that the young stars were originally formed in a dense star cluster outside the central half-parsec and transported to their present location by the effect of dynamical friction (Gerhard 2001). An intermediate-mass black hole (IMBH; a few thousand solar mass) may be required to stabilize the cluster core against its tidal disruption by the MBH before they move to the central half-parsec region (Hansen & Milosavljevic 2003; Kim et al. 2004; Gürkan & Rasio 2005; McMillan & Portegies Zwart 2003). Note that the existence of stellar disks in observations itself is not sufficient to differentiate these competing scenarios since a young stellar disk may form in the vicinity of the MBH in both of the scenarios. (For a review and more discussions on the pros and cons of these scenarios, see Genzel et al. 2003; Ghez et al. 2005; Paumard et al. 2006; Alexander 2005.)

Besides their young age, the peculiar orbital distribution of these stars also provides clues to their formation mechanism and the dynamical structure in the GC. It can also be used to differentiate various models. For example, in the in-spiraling star cluster scenario, the interactions between the central IMBH and the stripped young stars have been studied by Levin et al. (2005) and Berukoff & Hansen (2006). Although they were able to simulate the orbital features of stars on the thin disk, they had difficulties to account for the kinematic properties of those stars with eccentric orbits in the counterclockwise rotating disk. In this paper, we propose a dynamical model to account for the orbital distribution of the sub-parsec young stars in the GC. Rather than simultaneously investigating the formation mechanism of these young stars and their orbital distribution, we assume that all the sub-parsec young stars were formed in a clockwise rotating disk initially (e.g., due to instability or fragmentation of a massive accretion disk) with small eccentricities. We show in § 3 that, an isolated stellar disk by itself is unlikely to evolve from the presumed circular orbits in a thin disk to the currently observed multi-component orbital configuration. This inference is based on the determination that the timescale (e.g., the two-body relaxation timescale and the resonant relaxation timescale) for a single stellar disk to relax with respect to the background stars is usually substantially longer than the age of the young stars. Thus, the life-long eccentricity growth of the disk stars due to interactions among the stars is insignificant (not substantially larger than 0.2; Alexander et al. 2007). Therefore, the existence of young stars with high eccentricities and high inclination angles relative to the inner stellar disk requires an explanation, at least in the disk formation scenario of the young stars in the GC.

It is entirely plausible that, under the action of dynamical friction, a (dark) star cluster and/or an IMBH occasionally sink into the proximity of the GC. The (dark) star cluster (which may also have a central IMBH) or the IMBH plays the role of a massive perturber (or intruder), spiraling inward, inducing asymmetric perturbation of the gravitational potential and exerting torques on the disk stars. Interactions between the perturber and the disk stars, through either close encounters or some resonant interactions, may change the orbital distribution of the young stars. (In contrast to the in-spiraling young cluster hypothesis, the primary role of the cluster is to dynamically excite the eccentricity and inclination of the stars along its path rather than to directly deliver its own young stars to the GC.) In this paper, we develop dynamical models in order to examine whether the single stellar disk initially formed may evolve into the current observed orbital configuration, especially the eccentricity and inclination distribution, during and after the passage of an inward migrating massive perturber.

This paper is organized as follows. In § 2, we review the components observed in the GC. In § 3, we list some relevant dynamical timescales in the GC. In § 4, we describe dynamical models of gravitational interaction between the young stars in a primary disk and a massive perturber migrating inward from outside the stellar disk in the GC. We present the results of a set of numerical simulations of the dynamical models. Then we compare the model results with observations. Finally, conclusions are given in § 5.

2. COMPONENTS IN THE GC

We consider three components which contribute to the gravitational potential near the center of the Galaxy: a central MBH, a stellar cusp of old stars, and a population of young stars mentioned in § 1.

The MBH has a mass $M_{\rm BH} \simeq 3.6\times10^6\,{\rm M}_\odot$ (Ghez et al. 2005; Eisenhauer et al. 2005). The radius of the central MBH's sphere of influence is defined by

$$a_{\rm H} \equiv \frac{GM_{\rm BH}}{\sigma^2} \simeq 1.6\,{\rm pc}\; m_{\rm BH} \left(\frac{100\,{\rm km\,s^{-1}}}{\sigma}\right)^2, \qquad (1)$$

where G is the gravitational constant, σ is the one-dimensional velocity dispersion, and $m_{\rm BH} = M_{\rm BH}/(3.6\times10^6\,{\rm M}_\odot)$ in the GC.

The stellar cusp surrounding the young stars is mainly composed of old stars and stellar remnants including stellar-mass black holes and neutron stars. The mass density of the stellar cusp in the GC can be described by a power law (Genzel et al. 2003), i.e.,

$$\rho(r) = \rho_0 \left(\frac{r}{r_0}\right)^{-\alpha_i}, \quad i = 1, 2, \qquad (2)$$

where $\rho_0 = 1.2\times10^6\,{\rm M}_\odot\,{\rm pc}^{-3}$, $r_0 = 0.4\,{\rm pc}$, $\alpha_1 = 1.4\pm0.1$ for $r < r_0$ and $\alpha_2 = 2.0 \pm 0.1$ for $r > r_0$. This mass density gives the enclosed stellar mass in the inner cusp by

$$M_*(<r) = \frac{4\pi\rho_0 r_0^3}{3-\alpha_1}\left(\frac{r}{r_0}\right)^{3-\alpha_1}$$

$$= \epsilon M_{\rm BH} f_1(x), \quad if \quad r < r_0 \tag{3}$$

and

$$M_*(<r) = \frac{4\pi\rho_0 r_0^3}{3-\alpha_1} + \frac{4\pi\rho_0 r_0^3}{3-\alpha_2}\left[\left(\frac{r}{r_0}\right)^{3-\alpha_2} - 1\right] = \epsilon M_{\rm BH} f_2(x), \quad if \quad r > r_0, \tag{4}$$

where $\epsilon = \frac{4\pi\rho_0 r_0^3}{3-\alpha_1}/M_{\rm BH} \sim 0.16$, $x = r/r_0$, $f_1(x) = x^{3-\alpha_1}$ and $f_2(x) = \frac{3-\alpha_1}{3-\alpha_2}x^{3-\alpha_2} + \frac{\alpha_1-\alpha_2}{3-\alpha_2}$. The gravitational potential due to the cusp stars is

$$\Phi_*(r) = -\frac{GM_*(<r)}{r} + \frac{(3-\alpha_1)\epsilon GM_{\rm BH}}{r_0}\ln\left(\frac{r}{r_0}\right), \tag{5}$$

for $r > r_0$ and

$$\Phi_*(r) = -\frac{GM_*(<r)}{r} - \frac{(3-\alpha_1)\epsilon GM_{\rm BH}}{(2-\alpha_1)r_0}\left[1 - \left(\frac{r}{r_0}\right)^{2-\alpha_1}\right], \tag{6}$$

for $r < r_0$. The total potential due to the MBH and the cusp stars is $\Phi(r) = -\frac{GM_{\rm BH}}{r} + \Phi_*(r)$. Since the young stars interested in this paper mainly reside within the central half parsec and $r_0 = 0.4\,{\rm pc}$, for simplicity, we adopt $\alpha_2 = \alpha_1 \sim 1.4$ in our calculations below and use equations (3) and (5) even for $r > r_0$. Our main results will not be affected by slightly changing the value of the cusp slope.

3. SOME RELEVANT DYNAMICAL TIMESCALES IN THE GC

In this section, we estimate some dynamical timescales in the GC, which may be used for references or to justify the approximations in the dynamical models described in § 4.

- The orbital timescale of a star rotating around the central MBH is

$$T_{\rm orb} = 2\pi\sqrt{\frac{a^3}{GM_{\rm BH}}} = 1.5\times10^3\,{\rm yr}\; m_{\rm BH}^{-1/2}\left(\frac{a}{0.1\,{\rm pc}}\right)^{1.5}, \tag{7}$$

  where a is the orbital semimajor axis of the star.

- The local two-body relaxation timescale $T_{\rm relax}$ is given by

$$T_{\rm relax} \sim \frac{0.34\sigma^3}{G^2\rho_*\langle m_*\rangle\ln\Lambda} \sim \frac{2.0\times10^9\,{\rm yr}}{\ln\Lambda} m_{\rm BH}^{1/2}\frac{M_{\rm BH}}{M_*(<r)}\frac{1\,{\rm M}_\odot}{\langle m_*\rangle}\left(\frac{r}{0.4\,{\rm pc}}\right)^{3/2} \sim 1.2\times10^9\,{\rm yr}\; m_{\rm BH}^{1/2}\frac{10}{\ln\Lambda}\frac{1\,{\rm M}_\odot}{\langle m_*\rangle}\left(\frac{r}{0.4\,{\rm pc}}\right)^{-0.1}, \tag{8}$$

  where $\langle m_*\rangle$ is the mean stellar mass and ρ_* is the stellar density (e.g., Binney & Tremaine 1987; Alexander 1999). In the estimate of this timescale below (in Fig. 1), we set $\langle m_*\rangle \sim 1\,{\rm M}_\odot$ and $\ln\Lambda \sim 10$.

- The precession due to the stellar cusp: the stellar cusp (mentioned in § 2) may cause stars deviated from purely Keplerian motions and introduce apsidal precession of their orbits. This apsidal precession timescale can be estimated by

$$T_{\rm prec}^{\rm cusp} \sim \frac{M_{\rm BH}}{M_*(<r)}T_{\rm orb}(r) \sim 7.5\times10^4\,{\rm yr}\; m_{\rm BH}^{1/2}\left(\frac{r}{0.4\,{\rm pc}}\right)^{-0.1} \tag{9}$$

  with assuming $M_*(<r) \ll M_{\rm BH}$.

- Resonant relaxation timescales (see details in Rauch & Tremaine 1996; Hopman & Alexander 2006): in a timescale much longer than the orbital period and shorter than the apsidal precession timescale mentioned above, the star can be approximated by a fixed wire whose mass is the stellar mass, whose shape is a Keplerian ellipse, and whose linear density is inversely proportional to the local speed in the elliptical orbit. The wires precess on the timescale $T_{\rm prec}^{\rm cusp}$ and exert mutual torques which induce angular momentum relaxation. The cumulative effects of the torques result in the change of the absolute value of the angular momentum by a timescale of

$$T_{\rm relax}^{\rm res,S} \sim 3.56\times\frac{M_{\rm BH}+M_*(<r)}{\langle m_*\rangle}T_{\rm orb}(r) \tag{10}$$

  (hereafter the scalar-resonant relaxation timescale) or the change of the direction of the angular momentum vector by a timescale of

$$T_{\rm relax}^{\rm res,V} \sim 0.62\times\frac{M_{\rm BH}+M_*(<r)}{\langle m_*\rangle}\frac{T_{\rm orb}(r)}{N^{1/2}(<r)} \tag{11}$$

  (hereafter the vector-resonant relaxation timescale), where $N(<r) = M_*(<r)/\langle m_*\rangle$.

  The sub-parsec massive young stars is a different population from the major component (old stars with $\langle m_*\rangle = 1\,{\rm M}_\odot$ set here) in the Galactic center. We still take the above equations as the resonant relaxation timescales of the young stars, since their number and total mass are much smaller than the background old stars and the effect of the resonant relaxation on the young stars should mainly be due to the old stellar population (see the derivation in Rauch & Tremaine 1996).

- The apsidal precession due to the general relativity correction to the Newtonian equations of motion is given by (Misner et al. 1973):

$$T_{\rm GR} = \frac{ac^2(1-e^2)}{3GM_{\rm BH}}T_{\rm orb}(a) = 3.0\times10^7\,{\rm yr}\; m_{\rm BH}^{-3/2}(1-e^2)\left(\frac{a}{0.04\,{\rm pc}}\right)^{5/2}, \tag{12}$$

  where c is the speed of light.

- The Lense-Thirring precession timescale is given by (Misner et al. 1973)

$$T_{\rm LT} = \frac{2\pi a^3(1-e^2)^{3/2}}{2J}$$

$$= 2.2 \times 10^{10}\,\mathrm{yr}\; a_*^{-1} m_{\rm BH}^{-2} (1-e^2)^{3/2} \left(\frac{a}{0.04\,\mathrm{pc}}\right)^3, \quad (13)$$

where J is the angular momentum of the MBH and $a_* = J/(GM_{\rm BH}^2/c)$ is the dimensionless spin parameter of the MBH.

The above timescales are plotted as a function of the distance from the central MBH in Figure 1, with using the parameters of the observed stellar cusp described in § 2 (see a similar diagram in Hopman & Alexander 2006). As shown in Figure 1, the timescales $T_{\rm relax}$, $T_{\rm relax}^{\rm res,S}$, and $T_{\rm relax}^{\rm res,V}$ are all much longer than the stellar age $\tau_{\rm age}$ at $r > 0.04\,\mathrm{pc}$, which suggests that the spatial distribution of the original disk located at $0.04 - 0.5\,\mathrm{pc}$ cannot be erased through either two-body or resonant relaxation processes. The apsidal precession timescale $T_{\rm GR}$ is much longer than $\tau_{\rm age}$ for the stars at $a \gtrsim 0.1\,\mathrm{pc}$ and it is comparable to the age of the disk stars with moderate eccentricity at $a \lesssim 0.04\,\mathrm{pc}$. The apsidal precession may affect the orbits of the S-stars (since $T_{\rm GR} < \tau_{\rm age}$ for the S-stars), but it should be insignificant to the orbital evolution of the disk stars located at $a \sim 0.04 - 0.5\,\mathrm{pc}$. The Lense-Thirring precession is generally not important for those disk stars since $T_{\rm LT} \gg \tau_{\rm age}$ at $a \sim 0.04 - 0.5\,\mathrm{pc}$, but it may be important for the innermost two stars S2 (Levin & Beloborodov 2003) and S14 ($T_{\rm LT} \sim 4.1 \times 10^6 a_*^{-1}\,\mathrm{yr}$ for S2 $\sim 8.9 \times 10^6 a_*^{-1}\,\mathrm{yr}$ for S14). As seen from this Figure, the apsidal precession timescale due to the stellar cusp is much shorter than the age of the stars but much longer than their orbital period. This precession affects the secular orbital evolution of the young stars in the stellar disk.

According to the estimates of these relevant timescales (see Fig. 1), the disk stars in the GC may be described to be moving in a stellar cusp with a *smooth* potential (the apsidal precession due to the stellar cusp is naturally included in the description), and the effects of other precessions, apsidal precession due to the general relativity correction and the Lense-Thirring precession, may be neglected in the following calculations. In this paper, we do not pursue a study on the origin of the kinematics of the S-stars (with age of a few $10^7\,\mathrm{yr}$), for which the resonant relaxation, as well as the precession due to the general relativity correction and the Lense-Thirring precession, are involved (see also discussions in Hopman & Alexander 2006; Levin 2007) and a smooth potential may not be a good approximation any more.

In addition, if the young stars were formed in a gas disk, we assume that the gas disk was depleted quickly and gas drag is not important for their orbital evolution (damping the orbital eccentricity) at least for the two reasons based on observations: (1) most of the stars were formed in a short timescale $\lesssim 2\,\mathrm{Myr}$ compared to their age $6 \pm 2\,\mathrm{Myr}$; and (2) the MBH is accreting material via a rate around $10^{-6} - 10^{-5}\,\mathrm{M_\odot\,yr^{-1}}$ through a tenuous thick disk (e.g., Melia & Falcke 2001), which should not have any significant drag on the motion of the young stars.

4. MODEL AND NUMERICAL EXPERIMENTS

It is plausible that occasionally there may be a star cluster (and/or an IMBH) in-spiraling into the central region of the Galaxy (see also discussions in Perets et al. 2007). In this section, we study how the orbital configuration of the young stellar disk are affected by such a perturber. To isolate the problem, we first estimate how the orbits of the young stars is affected by a perturber rotating around the MBH at a fixed distance in § 4.1. We consider a range of inclination (from 0° to 180°) between the perturber's orbital plane and the stellar disk plane. In § 4.2, we illustrate how the orbital configuration of the stellar disk is affected by the inward-migration of a perturber.

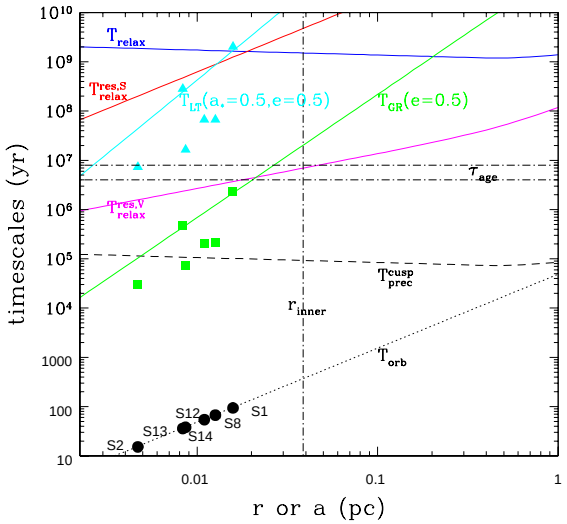

FIG. 1.— Relevant timescales for the young stars in the GC as a function of Galactocentric raidus r or semimajor axis of a stellar orbit a: the two-body relaxation timescale $T_{\rm relax}$ (blue solid line), the scalar-resonant relaxation timescale $T_{\rm relax}^{\rm res,S}$ (red solid line), the vector-resonant relaxation timescale $T_{\rm relax}^{\rm res,V}$ (magenta solid line), the Lense-Thirring precession timescale $T_{\rm LT}$ by assuming the dimensionless spin parameter of the MBH $a_* = 0.5$ and the eccentricity of the stars $e = 0.5$ (cyan solid line), the apsidal precession timescale due to the general relativity correction $T_{\rm GR}$ with assuming $e = 0.5$ (green solid line); the apsidal precession timescale due to the stellar cusp $T_{\rm prec}^{\rm cusp}$ (dashed line); and the orbital periods of the young stars $T_{\rm orb}$ (dotted line). For comparison, the age of those young stars $\tau_{\rm age} \sim 6 \pm 2\,\mathrm{Myr}$ and the inner radius of the clockwise disk $r_{\rm inner} \sim 1'' \sim 0.04\,\mathrm{pc}$ are marked by the dot-dashed lines. For reference, the relevant timescales for several S-stars (Eisenhauer et al. 2005; Ghez et al. 2005) with measured orbital parameters are also marked in this Figure (filled black circles: orbital periods; cyan triangles: Lense-Thirring timescales; green squares: apsidal precession timescales due to the GR correction). See detailed discussions in § 3.

4.1. *Perturbation on the stellar orbits due to a massive perturber at a fixed distance from the central MBH*

The orbital precession caused by the torque exerted by a massive perturber at a fixed distance from the central MBH (i.e., on a circular orbit) changes the inclination angles of the young stars, but not their eccentricities. In order for the clockwise rotating young stars in the inner region to retain their nascent disk's initial configuration, the oscillation amplitude of the inclination angle, induced by the nodal precession, needs to be small (say, $< 20°$; this number is roughly the maximum range of the estimated inclination angles of the young stars in the inner disk relative to the disk normal; Beloborodov et al. 2006). The oscillation amplitude should be small if the inclination angle between the orbital plane of the massive perturber and the stellar disk, denoted by β, is close

to 0°or 180°, but it can be large for other intermediate values of β unless the precession timescale is much longer than the stellar age.

Approximating the gravity of the perturber and the stars as rings, their nodal precession frequency is estimated to be (Nayakshin 2005; Nayakshin et al. 2006)

$$\omega_* = \frac{GM_{\rm p}}{(r^2+r_{\rm p}^2)^{3/2}}\frac{r_{\rm p}}{r}\frac{1}{\Omega_{\rm K}}I(\delta,\beta), \quad (14)$$

where $M_{\rm p}$ is the mass of the perturber which is much more massive than a young star, $\Omega_{\rm K}$ is the Keplerian angular frequency of the stars, $\delta = \frac{2r_{\rm p}r}{r_{\rm p}^2+r^2}$, $I(\delta,\beta) = \int_0^{2\pi}\frac{d\phi}{2\pi}\int_0^{2\pi}\frac{d\phi'}{2\pi}\frac{\sin\phi'\sin\phi}{[1-\delta(\cos\beta\sin\phi'\sin\phi+\cos\phi'\cos\phi)]^{3/2}}$, and $I(\delta,\beta) = I(\delta,\pi-\beta)$. Using equation (14), we show the precession timescale $\tau_{\rm precess} \equiv 1/\omega_* \propto 1/M_{\rm p}$ in Figure 2 with different parameters $r_{\rm p}$ and β. As seen from Figure 2, for a perturber with mass $M_{\rm p} = 10^4\,{\rm M}_\odot$ and located at a relatively large Galactocentric distance ($r_{\rm p} \sim 0.6\,{\rm pc}$; blue lines), the precession timescales in some region ($r \sim 0.5\,{\rm pc}$) may be smaller than the stellar age for some values of β and the orbital inclinations of the stars in this region may have substantial variations due to the nodal precession; but the precession timescale at $r \sim 0.04-0.15\,{\rm pc}$ is generally much longer than the stellar age and the initial coplanar structure of the inner disk can be well preserved for any values of β. If the perturber is located at a smaller Galactocentric distance ($r_{\rm p} \sim 0.2\,{\rm pc}$; red lines), the nodal precession timescale of the young stars at $r \sim 0.1\,{\rm pc}$ is much shorter than or comparable with their age if β is in the range ∼10°–80°(or ∼100°–170°); thus the orbital inclinations of the stars not only in the outer region ∼0.15–0.5 pc but also in the inner disk may have substantial variations or a warpness may be developed in the stellar disk due to the nodal precession (these qualitative estimates are confirmed by direct numerical calculations of the stellar orbital motion in § 4.2). If the perturber's orbit is almost perpendicular to the initial disk plane (red long-dashed line), the precession timescale for the young stars in the inner region is long enough compared to their age, and thus the inner disk may be not affected by the precession and its initial coplanar structure can be preserved. If the perturber orbit is nearly parallel to the disk plane, as mentioned in the paragraph above, although Figure 2 shows that the precession timescale is short compared to the stellar age, the disk configuration in the inner region may still be preserved since the oscillation of the normal to the stellar orbital planes around the normal to the perturber orbital plane is small. Thus, the preservation of the inner disk suggests that if the perturber with mass $10^4\,{\rm M}_\odot$ is located at $r_{\rm p} \sim 0.2\,{\rm pc}$, its orbit should be more likely to be parallel or perpendicular to the assumed primary disk. This result is also demonstrated in § 4.2 below. For a substantially smaller $M_{\rm p}$, the precession timescale $\tau_{\rm precess}$ can be long enough so that the inner disk may be maintained for a large range of β.

4.2. *Perturbation on the stellar orbits by an inward-migrating perturber*

In this subsection, we study how the background stellar orbits evolve as a massive nearby perturber migrating inward. For simplicity, we assume the perturber to be

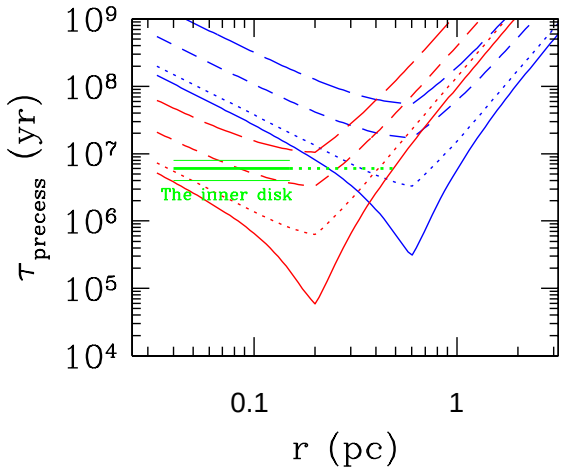

FIG. 2.— The timescales of the nodal precession of stellar orbits due to the torque exerted by a massive perturber with mass $M_{\rm p} = 10^4\,{\rm M}_\odot$ at a fixed distance from the central MBH $r_{\rm p}$. The stars are on nearly circular orbits with the Galactocentric distance r. The left (red) and right (blue) sets of lines are for a perturber located at $r_{\rm p} = 0.2\,{\rm pc}$ and $r_{\rm p} = 0.6\,{\rm pc}$, respectively. For each set, different line types represent different inclination angles β between the orbital plane of the massive perturber and that of the stellar disk [from top to bottom: $\beta = 85°$ (long-dashed lines), 75°(short-dashed lines), 45°(dotted lines), and 15°(solid lines)]. The age and position of the inner stellar disk ($\tau_{\rm age} \sim 6 \pm 2\,{\rm Myr}$ and $r \sim 0.04$–$0.15\,{\rm pc}$) observed in the GC are marked as solid green lines. The dotted green line illustrates the extension of the assumed original disk to $\sim 0.5\,{\rm pc}$. To preserve the coplanar structure of the stars in the region 0.04–0.15 pc not to be significantly affected by the nodal precession, the perturber should at least (i) be located at a far distance (e.g., $r_{\rm p} \sim 0.6\,{\rm pc}$), or (ii) have an orbit nearly parallel or perpendicular to the disk plane if the perturber is located at a small distance (e.g., $r_{\rm p} \sim 0.2\,{\rm pc}$), or (iii) have a substantially smaller mass. The orbits of the stars at the outer region (r ∼0.15–0.5 pc) can generally be affected by the nodal precession at some values of β unless the perturber mass is substantially smaller. See detailed discussion in § 4.1.

an IMBH with a point mass potential. If the perturber is a dark cluster, the gradually intensifying Galactic tidal effect is likely to induce the perturber to lose mass during its inward migration. We also consider the possibility that the perturber has a declining mass.

Before the perturber becomes bound to the central MBH, the perturber spirals into the Galactic center under the action of dynamical friction which induces a deceleration

$$\frac{d\vec{v}_{\rm p}}{dt} = -\frac{\vec{v}_{\rm p}}{\tau} - \nabla\Phi(r), \quad (15)$$

where the dynamical-friction timescale

$$\tau = t_{\rm df} = \frac{v_{\rm p}^3}{8\pi G^2 \ln\Lambda M_{\rm p}\rho(r)[{\rm erf}(X) - \frac{2X}{\sqrt{\pi}}exp(-X^2)]}, \quad (16)$$

$v_{\rm p} = |\vec{v}_{\rm p}|$ is the velocity of the perturber, $X = \frac{v_{\rm p}}{\sqrt{2}\sigma(r)}$, and $\ln\Lambda$ is the logarithm of the ratio of the maximum and minimum impact parameters and $\Lambda \simeq M_{\rm BH}/M_{\rm p}$ (Binney & Tremaine 1987). As the perturber or the IMBH migrates inward and forms a bound binary black hole (BBH) with the central MBH at $r_{\rm p} \simeq a_{\rm H}$ (see eq. 1), it continues to lose energy and angular momentum through dynamical friction. But, the influence of dynamical friction on the IMBH's orbit becomes less efficient as its orbital period decreases and its orbital velocity increases. After the BBH becomes hard at $a_{\rm h} = (M_{\rm p}/4M_{\rm BH})a_{\rm H} \simeq$

$0.004\,\mathrm{pc}\ m_{\rm BH}\left(\frac{M_{\rm p}/M_{\rm BH}}{0.01}\right)\left(\frac{100\,\mathrm{km\,s^{-1}}}{\sigma}\right)^2$, it loses energy mainly through three-body interactions with stars passing by its vicinity. The orbital decay timescale of a hard BBH in the GC is about $t_{\rm h}\equiv r_{\rm p}/\dot{r}_{\rm p}\simeq 6\times10^9\,\mathrm{yr}$ (see eq. 38 in Yu & Tremaine 2003). The gravitational radiation timescale of the BBH is longer than the Hubble time (see eq. 39 in Yu & Tremaine 2003) and it is unlikely to be significant in the spatial range of the BBH considered in this paper. During the transition stage (after the BBH becomes bound but before it becomes hard), the BBH's hardening timescale may be higher than the estimate from the dynamical friction timescale $t_{\rm df}(\sim 10^6\,\mathrm{yr}$ at 1 pc for $M_{\rm p}\sim 10^4\,\mathrm{M_\odot})$, as this process becomes less efficient, and it increases to that at the hard stage $t_{\rm h}$ as the IMBH migrates in (Yu 2002). Under the constraint placed on the distance between Sgr A* and the center of mass of the BBH (eq. 35 or Fig. 2 in Yu & Tremaine 2003), the mass of the secondary BH (or star cluster) $M_{\rm p}$ should be smaller than $\sim 0.03M_{\rm BH}$ if it is located at 0.3 pc and smaller than $\sim 0.08M_{\rm BH}$ if it is located at 0.1 pc. If the GC (or the central MBH) was formed through the assemblage of sinking star clusters (or IMBHs, which are considered to be candidates for the massive perturber in this paper), we can also infer their masses on the assumption that we are not living in a unique time. Such an argument would lead to a mass estimate for a typical perturber to be $\sim [M_{\rm BH}+M_*(<1\,\mathrm{pc})]\times 10^7\,\mathrm{yr}/10^{10}\,\mathrm{yr}\sim 5\times10^3\,\mathrm{M_\odot}$. Finally, star clusters with mass around $10^4\,\mathrm{M_\odot}$ are found within several tens pc from the GC. Based on these considerations, we adopt $M_{\rm p}=10^4\,\mathrm{M_\odot}$ as a fiducial mass for the massive perturber in general. We also consider the potential implications for other values of $M_{\rm p}$.

In the first set of simulations of stellar responses to a migrating perturber, its initial orbit is assumed to be nearly circular with a radius 1 pc. The path of inward migration follows equation (16), where the migration timescale τ is set to several different values $(10^6, 10^7, 10^8\,\mathrm{yr})$. The initial conditions of the perturber are set so that it attains an (almost constant) eccentricity ~ 0.02 after it moves sufficiently close to the MBH ($r_{\rm p}\lesssim 0.2\,\mathrm{pc}$). (In subsequent models, the potential implications for the higher values of the perturber's eccentricity are also considered. But we do not consider a highly eccentric orbit for the perturber, since the orbital decay of a dark cluster or a secondary BH via dynamical friction and three-body interactions with the central MBH and stars generally does not result in a highly eccentric orbit, e.g., with eccentricity $\lesssim 0.3$; Polnarev & Rees 1994; Quinlan 1996.) The orbital evolution of the perturber is shown in Figure 3. These results indicate that 15 Myr (or 10 Myr) would be required for the perturber to migrate inward from 1 pc (or 0.5 pc) to 0.1 pc if $\tau=10^7\,\mathrm{yr}$. In this paper, we do not address the interesting issue whether the migration of the perturber may be correlated with the formation of the young stars. We simply assume that the young stars formed throughout the disk prior to or during the migration of the perturber. Note that the time $t=0$ does not necessarily represent the time when the young stars formed.

We simulate the orbital evolution of 75 test particles as young stars, with the logarithm of their initial semi-major axes a distributed uniformly in the radial range lg(0.04 pc)–lg(0.5 pc). Each star moves independently in the potential of the central MBH, the inward-migrating IMBH, and the stellar cusp. We set the inclination of the perturber to zero and it does not change in the spherical gravitational potential of the cusp. Five sets of initial inclination angles of young stars i are chosen randomly in the range 0°–10°, 20°–30°, 80°–90°, 110°–120°, and 170°–180°, respectively. Their other orbital elements relative to the central MBH, such as the longitude of ascending node, argument of pericenter, and true anomaly, are chosen randomly in the range $[0°, 360°]$. The initial eccentricities e's of the orbits around the MBH are set to zero. But, they rapidly attain finite amplitudes, due to the gravity contributed by the stellar cusp. Given the position and velocity of a test particle at a given time, we can still define its time(or position)-dependent semimajor axis and eccentricity by assuming that the particle is on an elliptical orbit around the MBH at the appropriate time. In order to illustrate the change of the orbital configuration of a test particle, the angle of the orbital plane of each particle relative to its initial plane, θ, is used below, which may describe the observed inclination angles of the young stars relative to the observed inner disk (our conclusions do not change if the initial longitudes of ascending node of the particles in the simulations are set to be the same so that all the particles are initially on a thin disk). During their evolution, the orbits of two test particles with the same inclination angles do not generally lie on the same plane.

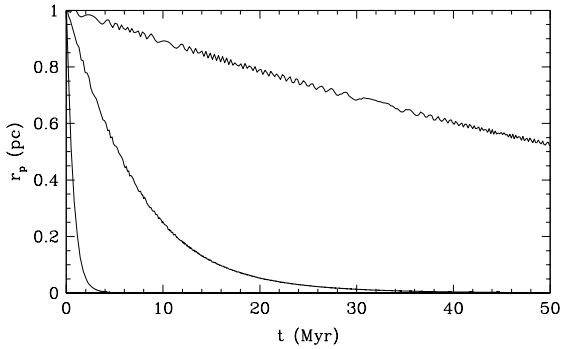

FIG. 3.— The orbital evolution of a perturber used in the dynamical model proposed in § 4.2. The perturber is initially on a nearly circular orbit at 1 pc and its evolution follows equation (15) with $\tau=10^8, 10^7, 10^6\,\mathrm{yr}$ from top to bottom.

We first show the simulation results for a model in which the perturber lies almost on the initial orbital plane of the disk stars ($i\in[0°, 10°]$). We set the perturber mass to be $M_{\rm p}=10^4\,\mathrm{M_\odot}$ and the migration timescale to be $\tau=10^7\,\mathrm{yr}$. From the simulation results, we find a range of stellar responses. For illustration purpose, it is useful to classify these responses into the following categories with representative cases shown in Figures 4–6.

A) Figure 4 shows the evolution of a test particle ($i\in[0°, 10°]$) which is captured into the 2:1 mean-motion resonance of inwardly migrating perturber, i.e., their orbital period ratio becomes 2:1 at $t/\tau\simeq 1$. After being captured, the particle migrates inward with the decaying perturber. During the resonant march, the particle retains an adiabatic invariant which for a $(p+q, p)$ mean-motion resonance is $C\equiv a^{1/2}[(p+q)-p(1-e^2)^{1/2}\cos i]$

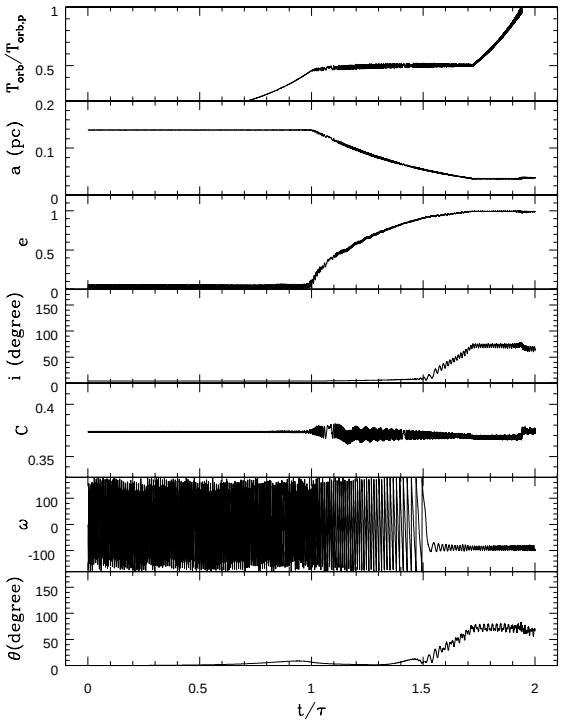

FIG. 4.— The orbital evolution of a test particle in the dynamical model proposed in § 4.2. The initial inclination angle of the particle is close to 0. From top to bottom, the panels show orbital period ratio to the perturber, semimajor axis, eccentricity, inclination angle to the orbital plane of the perturber, the quantity C defined in § 4.2, argument of pericenter, and the angle between the orbital plane of the particle and its initial orbital plane θ. The particle is first captured into the 2:1 mean-motion resonance and then released from the resonance but into the $\omega = \pm 90^\circ$ secular resonance.

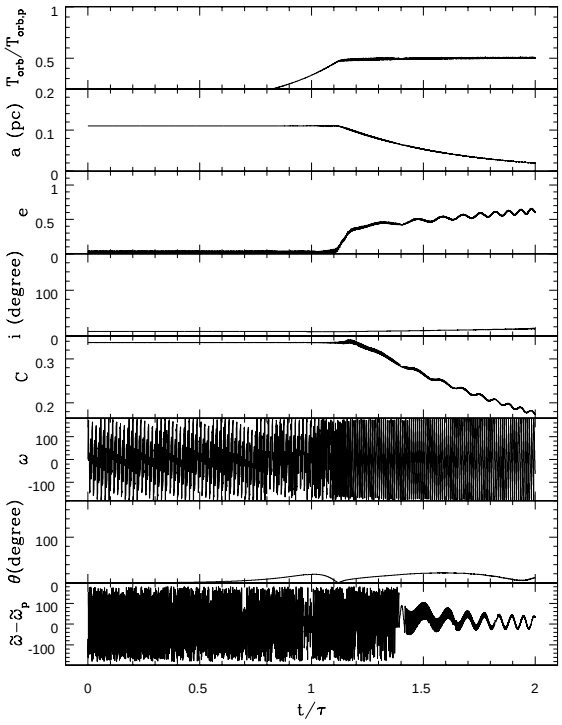

FIG. 5.— The orbital evolution of a test particle that is captured into the 2:1 mean-motion resonance and then into $\bar{\omega} - \bar{\omega}_{\rm p} = 0^\circ$ secular resonance, where $\bar{\omega} - \bar{\omega}_{\rm p}$ is the longitude difference of pericenter between the particle and the perturber.

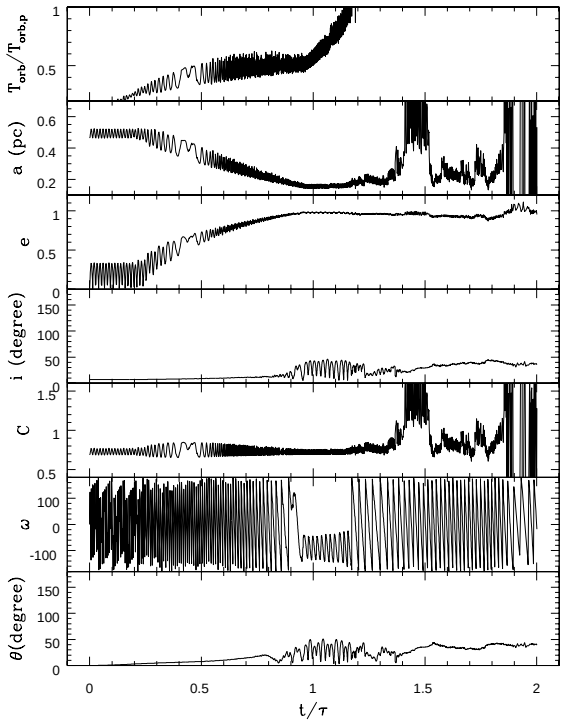

FIG. 6.— The orbital evolution of a test particle that initially follows the evolutionary pattern as that in Figure 4 and then is on an irregular orbit.

(Yu & Tremaine 2001). The magnitude of $p > 0$ and $q > -p$ are integers, and $p = q = 1$ for the inner (2,1) resonance (by "inner" refers to the resonances lie inside the perturber's orbit, i.e. with $a < a_{\rm p}$). For this adiabatic invariant, a reduction in the particle's semimajor axis during the migration can be compensated by an increase in its e and i. The results in Figure 4 indeed indicate a growth in the particle's eccentricity. When its eccentricity is sufficiently high (~ 0.9 at $t/\tau \simeq 1.5$), its inclination also grows. A comparison between the results of the two sets of simulations indicates that the inclusion of the stellar cusp in the gravitational potential promotes the elevation of the particle's inclination to a range between 0°–90°, rather than to a polar ($i = 90^\circ$) or a retrograde orbits ($i = 180^\circ$) around a point-mass potential (Yu & Tremaine 2001). The asymptotic inclination decreases with increasing fractional contribution of the stellar cusp mass to the gravitational potential. During the lifting of its inclination, the particle enters into a secular resonance with perturber's argument of the pericenter ω, librating around $\pm 90^\circ$. At an advanced stage of evolution ($t/\tau \sim 1.7$), the particle is released from the perturber's mean-motion resonance when it attains relatively large eccentricity and inclination. But, the particle retains its secular resonance ($\omega \sim \pm 90^\circ$) with the perturber which prevents close encounters between them. Consequently, the orbit of the particle is stable on the timescale of our integration ($\sim 5 \times 10^2$ initial orbital periods of the perturber).

B) Figure 5 illustrates the evolution of second representative particle with a similar $i \in [0^\circ, 10^\circ]$ but have a different initial location to that in the previous example. The initial evolution of this particle is generally the same as that in the previous model (Figure 4). The particle is captured into the perturber's mean-motion resonance of

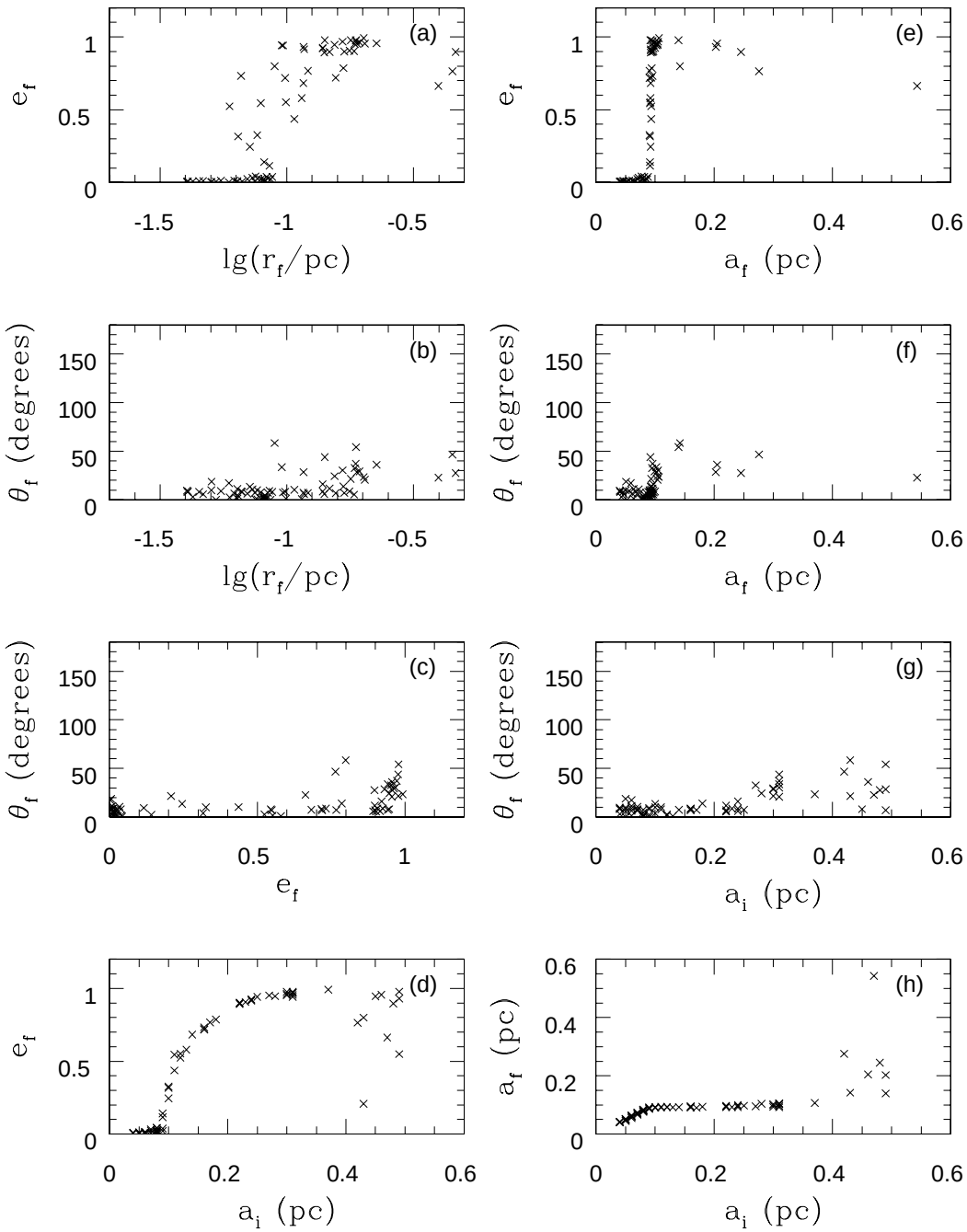

FIG. 7.— Orbital distribution of simulated test particles when the perturber with mass $10^4\,M_\odot$ migrates to 0.15 pc (denoted by the subscript "f"; the initial values of their orbital parameters are denoted by the subscript "i"). The initial inclination angles of the particles to the perturber plane are in the range $[0°, 10°]$. Note that the distance to the central MBH r_f is generally different from the semimajor axis of the particle a_f due to the non-zero eccentricity e_f. See § 4.2.

the perturber at $t/\tau \gtrsim 1.1$ (see Figure 5). At $t/\tau \sim 1.4$, the test particle enters into a state of secular resonance with the perturber such that the difference of their pericenter longitude $\eta \equiv \bar{\omega} - \bar{\omega}_{\rm p}$ (where $\bar{\omega} = \Omega + \omega$ and Ω is the longitude of ascending node) librating around 0. During this phase, the quantity C is no longer an invariant. The capture of the particle into this perturber's secular resonance can be understood through the evolution of the difference between the precession rates of the perturber and the test particle, which may be described by $d\eta/dt = A_1 + A_2\cos(\eta)$ (Nagasawa, Lin & Ida 2003). The right-hand side of this evolution equation includes the contribution from the precession of the test particle induced by the secular interaction with the perturber and also the contribution from the precession of both the perturber and the test particle induced by the stellar cusp. As the perturber and the test particle migrate inward, both of these contributions evolve with time. At some point during the course of migration, $A_1 \ll A_2$ and the longitude difference of pericenter librates around $\eta = 0$ (or 180°). The eccentricity ratio of the test particle and the perturber $e/e_{\rm p}$ [which evolves as $d(e/e_{\rm p})/dt \propto \sin\eta$; Nagasawa, Lin & Ida 2003] also librates around an equilibrium value. As the test particle continues to migrate inward with the perturber, it may retain the state of secular resonance but the equilibrium value of the ec-

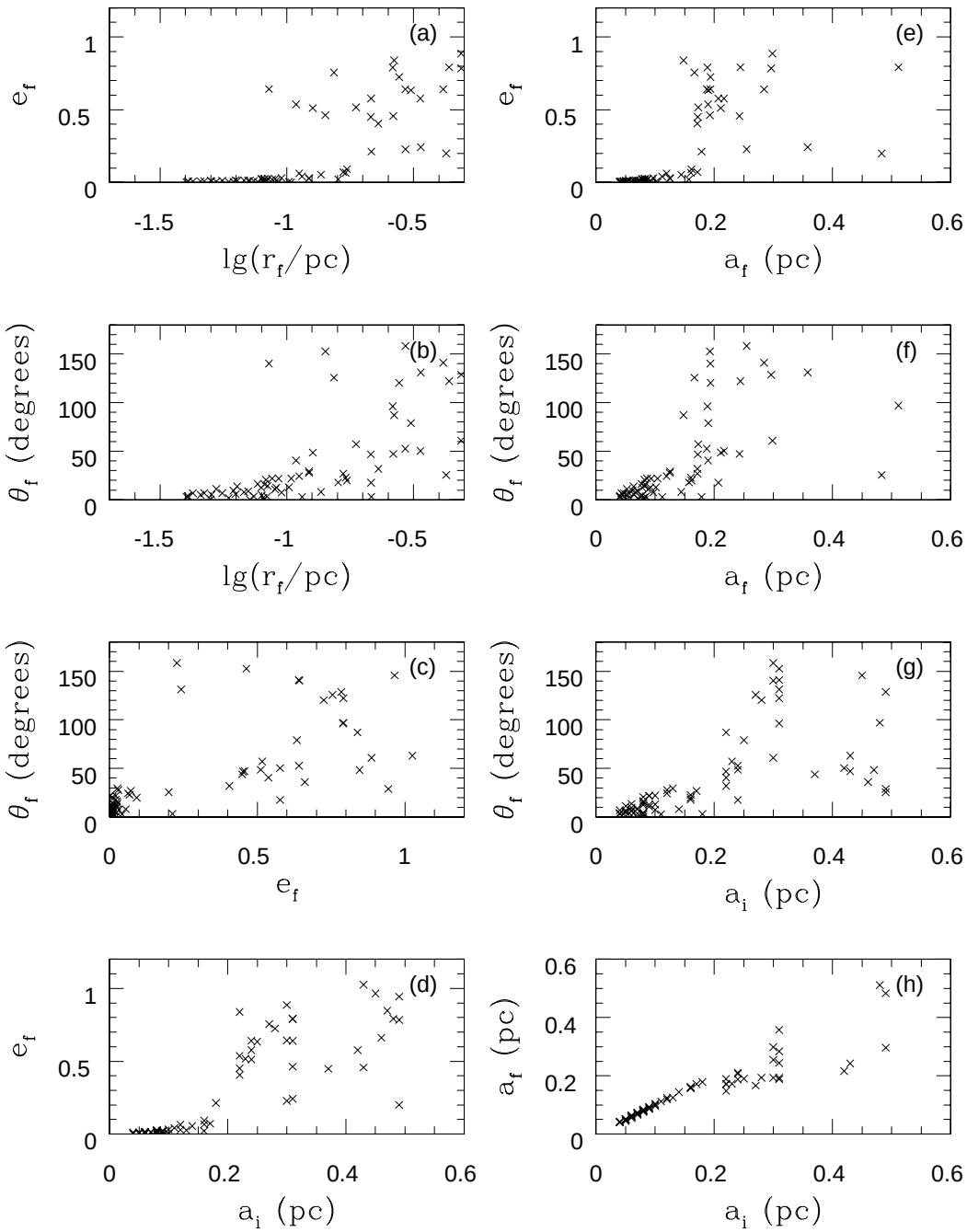

FIG. 8.— Orbital distribution of simulated test particles with initial inclination angles $i \in [80°, 90°]$, when the perturber with mass $M_{\rm p} = 3 \times 10^4\,{\rm M}_\odot$ migrates to $r_{\rm p} = 0.3\,{\rm pc}$. Other initial conditions are the same as those in Figure 7.

centricity ratio changes as the Hamiltonian of the system evolves. Similar secular resonance was discussed in Nagasawa, Lin & Ida (2003), where the depletion of a protostellar disk around a planetary system causes the change of the precession rates of the system. In this paper, the change of the precession rates is caused by the migration of the system in a stellar cusp.

C) Figure 6 shows a third example of the evolution of a test particle ($i \in [0°, 10°]$), which has a similar evolutionary pattern as that in Figure 4 at $t/\tau \lesssim 1.4$ and is on an irregular orbit afterwards.

The above three categories essentially convert the entire domain of stellar responses. But the actual outcome of the perturber's passage sensitively depends on the particles' initial orbital parameters. In this set of simulations, most of the particles with initial semimajor axis in the range 0.2–0.5 pc fall into case C, and the stars with smaller semimajor axes generally fall into case A and a few in case B. Figure 7 shows the distribution of the orbital parameters of the test particles. In this figure, the subscripts "i" and "f" of various variables represent their initial and final values, respectively. For the "final" values, we refer to those when the perturber migrates to $r_{\rm p} = 0.15\,{\rm pc}$ ($t/\tau \simeq 1.1$). (Note that the value of $r_{\rm p}$ is an instantaneous position of the perturber, and the perturber does not necessarily stop there but continues to migrate inward under the action of dynamical friction with time going on.) As seen from Figure 7(g), (d),

and (h), the semimajor axes, eccentricities, and inclination angles of particles with small initial semimajor axis ($a_i \lesssim 0.1\,\mathrm{pc}$) are not greatly affected by the migration of the perturber. Test particles with initial semimajor axes in the range 0.1–0.3 pc have essentially the same final semimajor axes ($\sim 0.1\,\mathrm{pc}$) because these particles are captured into the 2:1 mean-motion resonance and forced to migrate with the perturber during its orbital evolution. As seen from panels (d)–(g), their eccentricities and inclinations may be excited to high values. Panel (c) indicates that the test particles with high inclination angles generally have high eccentricities. The particles with the same semimajor axes may have different instantaneous distances r_f from the central MBH due to the non-zero eccentricity e_f. Panels (a) and (b) show the distribution of the eccentricities and inclination angles versus the distances. Panel (a) indicates the tendency that the eccentricities of the test particles are low at the small radii and high at the large radii. Panel (b) indicates that the stellar disk may be maintained at the inner radii [$\lg(r_f/\,\mathrm{pc}) \lesssim -0.8$] and the test particles at the outer radii have high inclination angles relative to the inner disk. Most particles with initial semimajor axes larger than $\sim 0.35\,\mathrm{pc}$ are captured into 2:1 resonance during the early stages of the perturber's evolution but they are released from the resonance and attained irregular orbits after the perturber has migrated inside $r_\mathrm{p} = 0.15\,\mathrm{pc}$.

We also check the dependence of the final orbital distribution on the perturber's position r_p, mass M_p, and eccentricity. For a smaller $r_\mathrm{p} = 0.1\,\mathrm{pc}$, the inclination angles and eccentricities of the stars at the inner radii ($r_f < 0.1\,\mathrm{pc}$) may also be excited to high values and the inner disk can no longer be maintained. For a larger $r_\mathrm{p} = 0.3\,\mathrm{pc}$, although the 'final' eccentricity distribution is qualitatively similar to those shown in Figure 7, but the inclination angles θ_f cannot be excited beyond 20°. A relatively low-mass perturber (e.g., $M_\mathrm{p} = 10^3\,\mathrm{M}_\odot$) cannot significantly excite the inclination angles, either, although it can excite some particles' eccentricities to high values by capturing them into the 2:1 or 3:2 mean-motion resonance. An increase in the perturber mass (e.g., $M_\mathrm{p} = 3\times10^4\,\mathrm{M}_\odot$) enhances its secular perturbation and widens its mean-motion resonances. So does an increase in the perturber's eccentricity or an increase in the test particles' initial eccentricities of the test particles. In these cases, some particles are captured into mean-motion resonances other than the 2:1 resonance, such as, the 3:2, 3:1, or 4:1 resonance. Some particles may transit from one mean-motion resonance to another mean-motion resonance during their orbital evolution. Relatively more particles are captured into secular resonance $\bar{\omega} - \bar{\omega}_\mathrm{p} = 0°$ or 180°.

We now consider the possibility that the perturber migrates to the proximity of the stellar disk on a highly inclined orbit. We show the case that the initial disk plane is almost perpendicular to the perturber orbital plane in Figure 8, for which $M_\mathrm{p} = 3\times10^4\,\mathrm{M}_\odot$ and $r_\mathrm{p} = 0.3\,\mathrm{pc}$. In this case, most of the main features of the distribution in Figure 7 are preserved, including the maintenance of a coherent inner stellar disk with $\theta_f \lesssim 20°$. The angles of the final orbital plane of the stars relative to their initial disk plane θ_f have a much larger range 0°–180° than those shown in Figure 7. Figures 9 and 10 illustrate

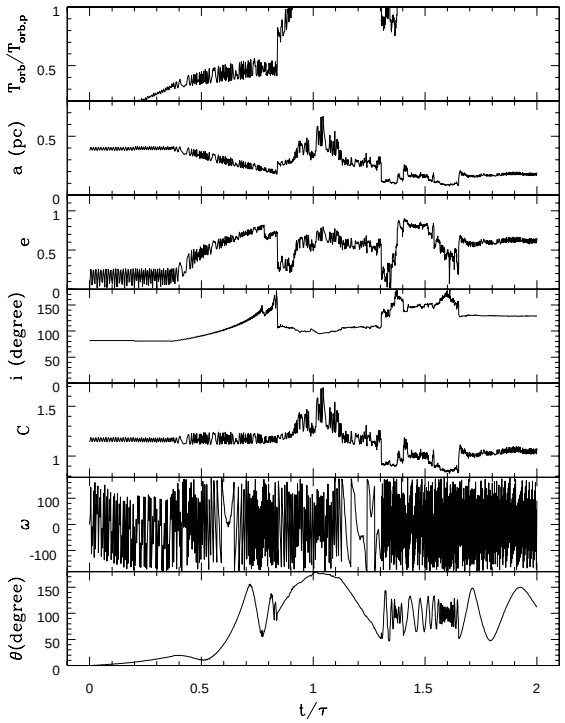

FIG. 9.— The orbital evolution of a test particle with initial inclination angle close to 90°. The particle is first captured into the 2:1 mean-motion resonance and then is on an irregular orbit.

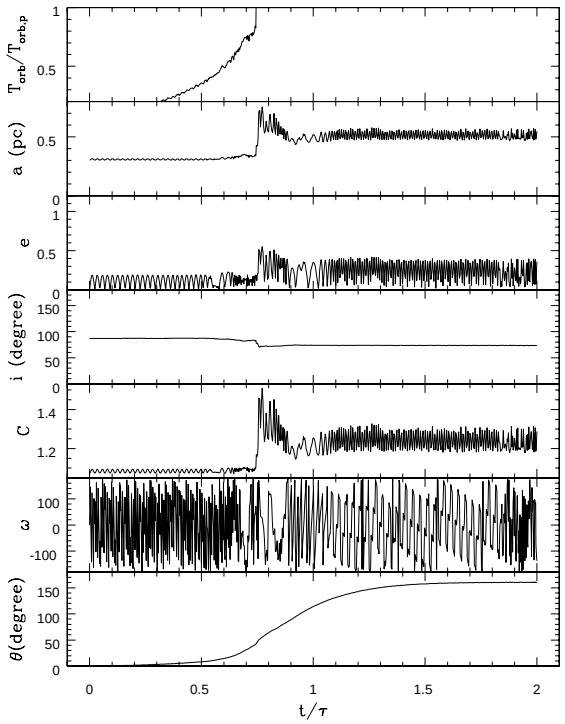

FIG. 10.— The orbital evolution of a test particle with initial inclination angle close to 90°. Although the inclination angle of the particle relative to the perturber orbital plane i changes little, the angle of the particle orbital plane to its initial orbital plane θ changes significantly due to the nodal precession in the gravitational potential of the stellar cusp and the change of the inclination angle from an initial value close to 90° to $\sim 70°$ at $t \sim 0.75\tau$ caused by a close encounter. The angle θ is almost constant or does not oscillate after $t/\tau \sim 1.5$ because the perturber has migrated into the inner region and does not have significant effects on the orbital evolution of the outside particle anymore.

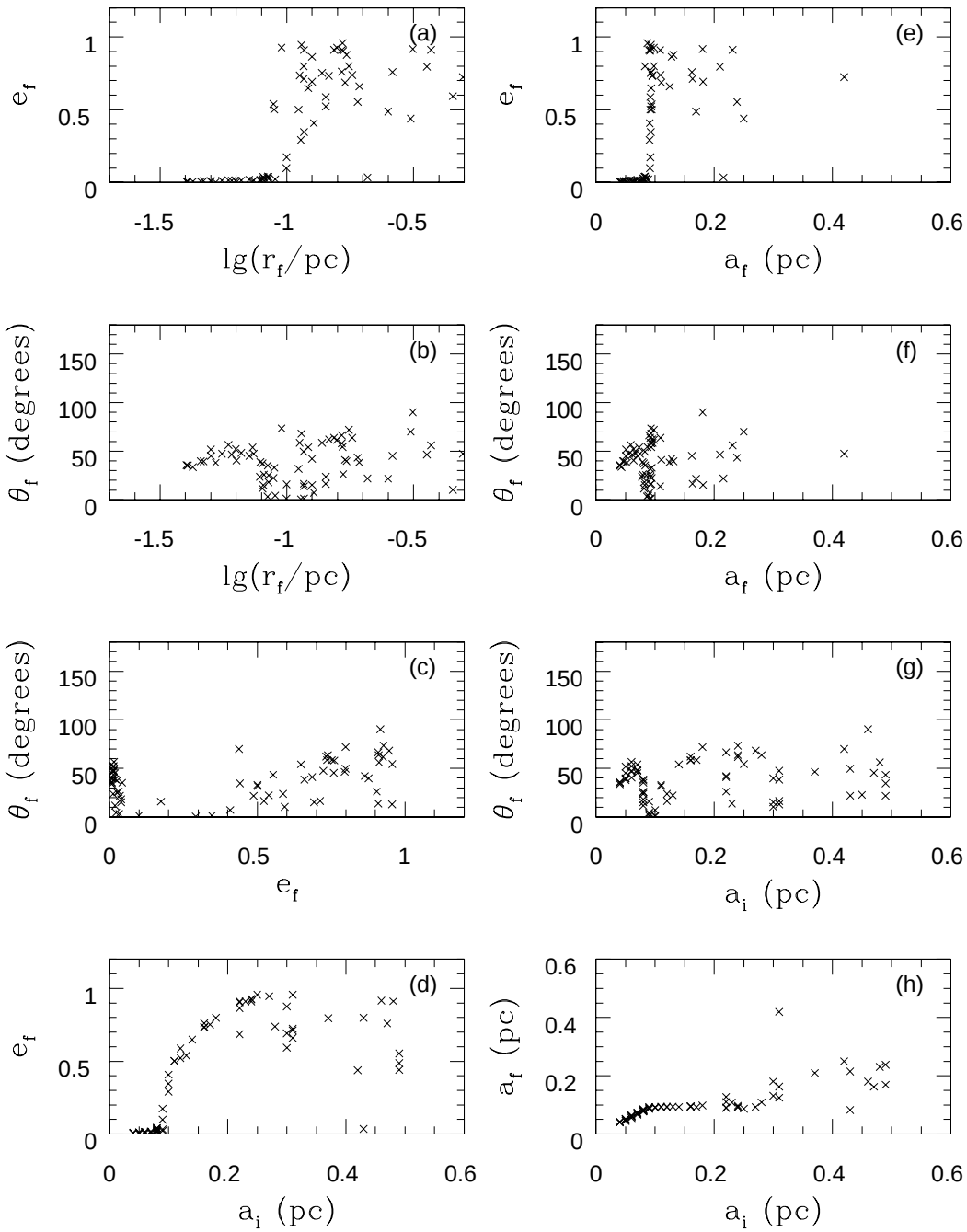

FIG. 11.— Orbital distribution of simulated test particles with initial inclination angles $i \in [20°, 30°]$ when the perturber with mass $10^4\,M_\odot$ migrates to 0.15 pc. Other initial conditions are the same as those in Figure 7.

two representative particles' orbital evolution. In Figure 9, after the particle is captured into the perturber's 2:1 mean-motion resonance (or 3:2 resonance for some other particles), both its eccentricity and its inclination also increase as the particle migrates inward. The magnitude of C is an adiabatic invariant at $t/\tau \lesssim 0.8$ and the particle is on an irregular orbit after it undergoes a close encounter with the perturber at that epoch. In Figure 10, the inclination angle of this particle i changes little during the evolution; but after i flips from an initial value close to 90° to $\sim 70°$ because of its close encounter with the perturber at t/τ ∼0.7–0.8, the angle between the orbital plane of the particle and its initial orbital plane changes significantly due to the nodal precession of the particle orbital plane. The excitation of the eccentricities of the test particles shown in Figure 8 results from their capture into mean-motion resonances and close encounters with the perturber. In addition to resonance capture and close encounters, nodal precession due to the perturber also results in the excitation of the inclination angles θ. The distribution of the final semi-major axes of the particles in the outer region (e.g., see $a_f > 0.15$ pc in Fig. 8e) is broader than that shown in Figure 7 due to the scattering through close encounters with the perturber and wider resonances that they are captured into.

We also calculate the orbital distributions of the particles if their initial inclination angles to the perturber's

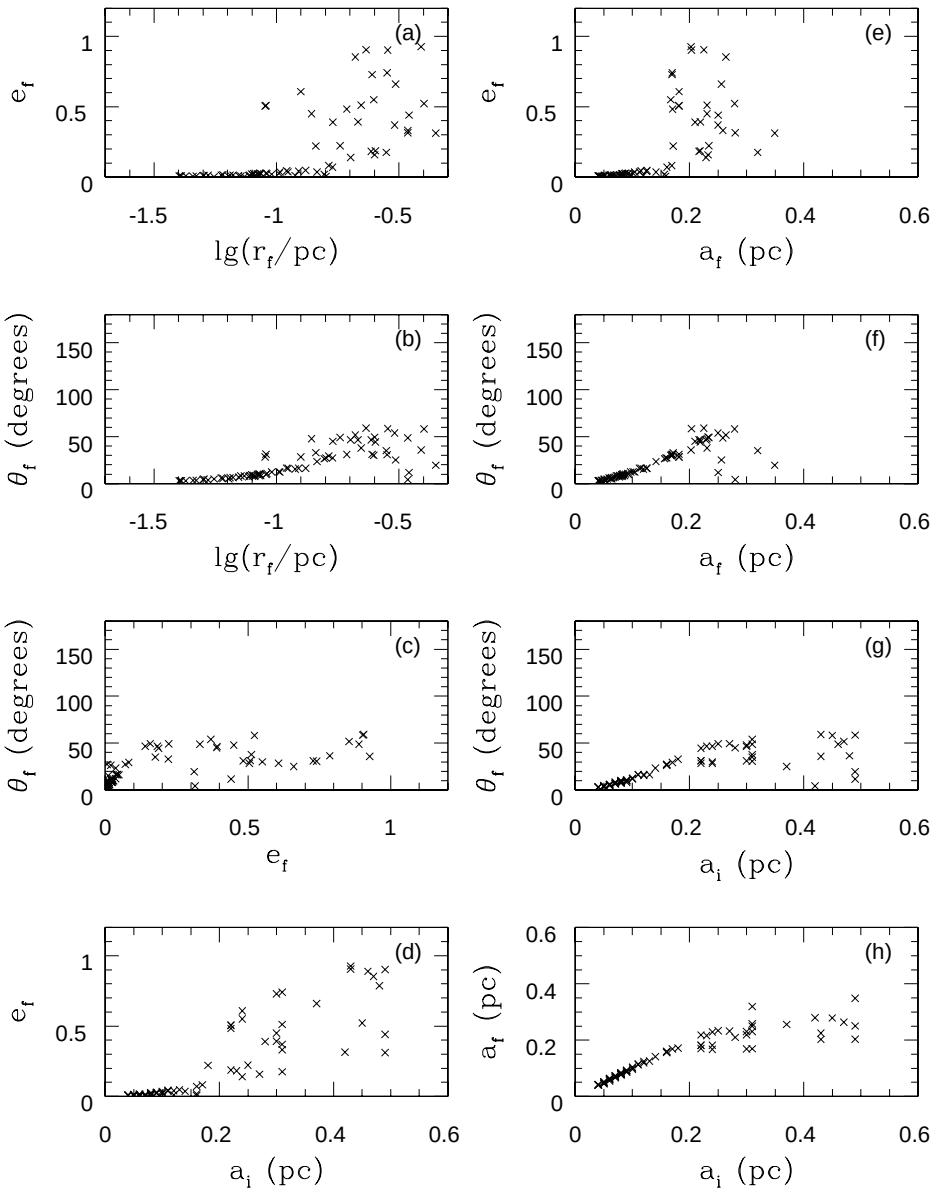

FIG. 12.— Orbital distribution of simulated test particles with initial inclination angles $i \in [20°, 30°]$ when the perturber with mass $5 \times 10^3\,M_\odot$ migrates to 0.3 pc. Other initial conditions are the same as those in Figure 7.

orbital plane i are in the range 20°–30°, 110°–120°, and 170°–180°, respectively. For the cases of initial $i \in [20°, 30°]$ and $i \in [110°, 120°]$, if the perturber migrates to a position $r_p = 0.15$ pc, the stars in the inner radii cannot be maintained on a disk (with θ_f up to 50° or 120°, e.g., see Fig. 11) due to the nodal precession of the particles' orbital planes, which is consistent with our discussion in § 4.1. If the perturber has a smaller mass and migrates to a relatively outer position (e.g., $M_p = 5 \times 10^3\,M_\odot$ and $r_p = 0.3$ pc), the angles θ_f of the inner stars can be small (e.g., $\lesssim 20°$), but a warpness may be developed in the disk (the warpness is not indicated by observations so far). For the case of initial $i \in [20°, 30°]$ (see Fig. 12), both the eccentricities and inclinations of the stars at the outer region can be excited up due to capture into mean-motion resonances, close encounters with the perturber, and nodal precessions. But the eccentricities cannot be sufficiently excited up in the case of initial $i \in [110°, 120°]$ (e.g., with $e_f \lesssim 0.6$), because our simulations show that they are less likely to be captured into mean-motion resonances compared to the case of $i \in [20°, 30°]$ or that their mean-motion resonances are more likely to be unstable and affected by close encounters with the perturber. A relatively higher perturber mass may increase the excited eccentricities due to close encounters, but it also induces larger nodal precession of stars at the inner radii.

For the case of initial $i \in [170°, 180°]$, the inner stars may be maintained on a disk and on nearly circular orbits. The angles θ_f of the stars with large initial semi-major axes (e.g., $a_i > 0.3$ pc) can be excited up to 50°, and their eccentricities can also be excited up. But many excited particles have large a_f (e.g., $\gtrsim 0.5$ pc) and the excited eccentricity e_f of the particles at $r \sim 0.15 - 0.5$ pc are not high enough (e.g., $\lesssim 0.6$) compared to the observations shown in Figure 13. In this case, both of the inclination and eccentricity excitations come mainly from close encounters with the perturber.

If the perturber is a dark cluster (with a central IMBH), its orbital decay may be accompanied with mass

loss induced by the strong external tidal potential. Our simulations indicate that for the same initial perturber mass, a decrease in the perturber mass during its orbital decay may make the inner stellar disk more likely to be preserved.

We also test the effects of different perturber-migration timescales. For longer migration timescales (e.g., 5 Myr or 10 Myr), the main results are generally not affected. Note that a very large ($\gg 10$ Myr) migration timescale is not compatible with the estimated age of the young stars. For a substantially shorter migration timescale (e.g., $\tau = 1$ Myr), the inward-migration of the perturber is too fast for some particles to be captured into the mean-motion resonance and the excitation of the eccentricity and inclination becomes insufficient.

4.3. *Comparison with observations and discussions*

The numerical models in § 4.2 simulate the interaction between a disk of stars with nearly circular orbits and an inward-migrating perturber. Provided the perturber's orbit is either nearly coplanar (in corotating directions) or essentially overhead, the young stars at the outer region generally attain high eccentricities (up to unity), while those at the inner region retain low eccentricities. In addition, the young stars at the outer region tend to have a large range of inclination angle relative to the disk, while those in the inner region roughly remain in the initial disk (see panels a and b in Figs. 7 and 8).

These features are consistent with the observed features of the orbits partly listed in the items (a), (b) and (c) in § 1. In order to make a quantitative comparison with observations, we plot the eccentricities of the young stars in the GC versus their observed distance to the central MBH in Figure 13 (the data are adopted from Paumard et al. 2006). This figure indeed indicates a correlation that the stars in the outlying regions of GC have high eccentricities (close to 1) while the inner ones only have moderate eccentricities. This apparent correlation is reproduced in our model as shown in panel (a) in Figures 7 and 8. Note that the low eccentricity of the test particles in the inner region (with $r_f < 0.15$ pc) preserved (panel a in Figs. 7 and 8), which appears inconsistent with the observational range of $0.2 - 0.4$ (Fig. 13). However, the eccentricities of the young stars at the inner region may relax to the observed values due to the interactions among the stars as shown in Alexander et al. (2007), which are not considered in § 4. An N-body numerical simulation of the model proposed in this paper would provide a quantitative consistency check. Our calculations in § 4.2 show that the inclination of the stars in the outer region relative to the inner disk is less excited for a nearly coplanar perturber orbit (only up to $\sim 50^\circ$) than for an overhead perturber orbit. The inclination angles of the outer stars are not well determined in observations, but if they have higher inclinations (e.g., $\sim 110^\circ$ in item a in the § 1), the perturber would be more likely to be on an overhead orbit. Precise determination of the inclination of the stars in the outer region will be important to distinguish the inclinations of the perturber.

In the in-spiraling-cluster scenario (briefly discussed in § 1 to account for the origin of the young stars), we note that, within a limited dispersion, the eccentricities of the tidally disrupted stars are usually comparable to that

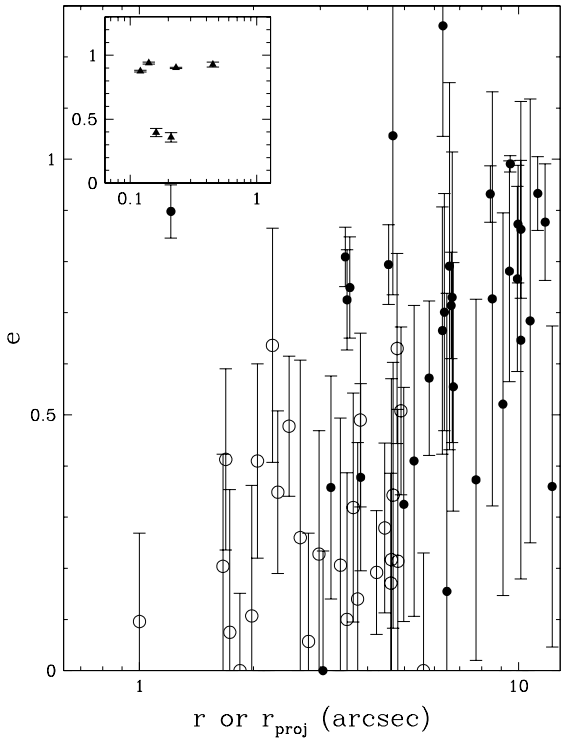

FIG. 13.— The eccentricities of the young stars in the GC versus their observed distance to the central MBH. The open circles represent those stars having the measurements of the (three-dimensional) distance (r). The solid circles represent those stars only having the measurements of the projected distance ($r_{\rm proj}$). The inset shows several S-stars which have the eccentricity estimates. The figure shows a tendency that the outer stars have high eccentricities (close to 1) while the inner ones (with exclusion of the S-stars) only have moderate eccentricities. The data used here are adopted from Paumard et al. 2006. Using the Spearman correlation analysis, we find a quite strong correlation between the eccentricity and the projected distance and the correlation coefficient between the eccentricity and the projected distance is $R_S = 0.58$ with $P_{R_S} = 8 \times 10^{-7}$.

of the in-spiraling star cluster. The dominant component of the velocity vector of the dispersed stars is their co-moving motion with the cluster and the velocity of the stars relative to the center of the cluster is relatively small (Berukoff & Hansen 2006). Therefore, it is unlikely that the observed eccentricity distribution of the young stars shown in Figure 13 can be produced by a disrupted single in-spiraling young star cluster. In order to reproduce the observed velocity distribution, the disruption of a second hypothetical in-spiraling young star cluster may be required (e.g., Berukoff & Hansen 2006). Such a scenario seems contrived because the coeval nature of the young stars also requires these clusters to be formed simultaneously.

The model we analyzed here is different from that two in-spiraling star cluster scenario. In our model, all the young stars are initially in a single disk and then the orbits of the young stars in the outer region of the disk are perturbed by an inward-migrating (dark) star cluster or an IMBH onto high eccentricity and high inclination orbits.

Figures 7, 8 and 12 (e) and (f) indicate one of the features of our model that because they are captured into mean-motion resonance, some test particles have nearly the same semimajor axes with widely different eccentricities. The particles captured into the resonance are likely

to have close encounters with each other, which should modify the orbital distribution obtained here. Our preliminary N-body results show that some of the particles captured into the mean-motion resonance may then be scattered out of the resonance. Nevertheless, a substantial number of particles still attached to the resonance. The main conclusion derived in Figs. 7 and 8 are not expected to change significantly. The existence of resonant stars, if can be extracted from the observational data, would not only provide an important check for our model but also strongly signify the possible presence of an IMBH in the GC.

Our simulation results show that the inclination angles of the young stars at the outer region of the initial disk may be excited up to different values as the perturber migrating inward. The excited stars cannot form a coherent secondary disk in this model. The formation of a secondary disk is also challenging in the in-spiraling cluster scenario (Berukoff & Hansen 2006). In any event, observational evidence of the existence of a secondary disk remains controversial.

5. CONCLUSIONS

We studied the dynamical evolution of a young stellar disk surrounding the MBH in the GC and perturbed by an inward migrating IMBH or a (dark) star cluster hosting an IMBH. Our numerical simulations show that the orbits of the young stars in the disk may be significantly modified from the outside in by the perturber. If the perturber has a low inclination angle to the initial disk, its migration from a region outside to $\sim 0.15\,\mathrm{pc}$ may excite the eccentricities (up to unity) and the inclination angles of stars in the outer (0.2–0.5 pc) regions by capturing them into its mean-motion and secular resonances, forcing them to migrate with it, and/or closely encountered with them. Stars interior to this region preserve their initial coplanar structure. The overall dynamical distribution of the stars reproduces that observed on sub-parsec scale around the GC, i.e., an inner disk surrounded by a torus of highly eccentric and inclined stars. If the perturber migrates to $\sim 0.3\,\mathrm{pc}$ on an orbit which is nearly perpendicular to the initial disk, the stars in the outer regions can still be excited to highly eccentric and inclined orbits through resonant capture and nodal precession induced by and close encounters with the perturber. The inclinations can be excited to be in a larger range in the perpendicular case than those excited in the low-inclination case. In the perpendicular case, the stars in the inner region can also retain their low eccentricities and remain on the initial disk. These results reproduce many features of the observed orbital distribution of subparsec young stars. Note that the predicted position for the perturber here is an instantaneous value, and the perturber does not necessarily stop there but continues to migrate inward under the action of dynamical friction with time going on.

Further measurements of the orbital parameters of the young stars in the GC (e.g., semimajor axes, eccentricities, and inclination angles) would provide important tests for the model proposed in this paper. It would also be useful to distinguish various scenarios proposed to account for the formation of the young stars. An important confirmation for the model proposed in this paper is the discovery of a perturber [either an IMBH or a (dark) cluster hosting an IMBH] with a mass in the range $3\times10^3-3\times10^4\,\mathrm{M}_\odot$ at $r\sim0.15-0.3\,\mathrm{pc}$ with an orbital plane which is either nearly parallel or perpendicular to the inner disk plane.

We have benefited from discussions with Scott Tremaine. This work is supported by NASA (NAG5-12151, NNG06-GH45G), JPL (1270927), NSF(AST-0507424). Q.Y. acknowledges initial support from NASA through Hubble Fellowship grant HST-HF-01169.01-A awarded by the Space Telescope Science Institute, which is operated by the Association of Universities for Research in Astronomy, Inc., for NASA, under contract NAS 5-26555.

REFERENCES

Alexander, R. D., Begelman, M. C., & Armitage, P. J. 2007, ApJ, 654, 907
Alexander, T. 1999, ApJ, 527, 835
Alexander, T. 2005, Phys. Rep., 419, 65
Beloborodov, A. M., Levin, Y., Eisenhauer, F., Genzel, R., Paumard, T., Gillessen, S., & Ott, T. 2006, ApJ, 648, 405
Berukoff, S. J., & Hansen, B. M. S. 2006, ApJ, 650, 501
Binney, J., & Tremaine, S. 1987, Galactic Dynamics (Princeton, NJ: Princeton University Press)
Eisenhauer, F., et al. 2005, ApJ, 628, 246
Genzel, R., et al. 2003, ApJ, 594, 812
Gerhard, O. 2001, ApJ, 546, L39
Ghez, A. M., et al. 2003, ApJ, 586, L127
Ghez, A. M., et al. 2005, ApJ, 620, 744
Goodman, J. 2003, MNRAS, 339, 957
Gürkan, M. A., & Rasio, F. A. 2005, ApJ, 628, 236
Hansen, B. M. S., & Milosavljevic, M. 2003, ApJ, 593, L77
Hopman, C., & Alexander, T. 2006, ApJ, 645, 1152
Kim, S. S., Figer, P. F., & Morrison, M. 2004, ApJ, 609, 123
Levin, Y. 2007, MNRAS, 374, 515
Levin, Y., & Beloborodov, A. 2003, ApJ, 590, L33
Levin, Y., Wu, A., & Thommes, E. 2005, ApJ, 635, 341
Nagasawa, M., Lin, D. N. C., & Ida, S. 2003, ApJ, 586, 1374
Nayakshin, S. 2005, MNRAS, 359, 545
Nayakshin, S., Dehnen, W., Cuadra, J., & Genzel, R. 2006, MNRAS, 366, 1410
McMillan, S. L. W., & Portegies Zwart, S. F. 2003, ApJ, 596, 314
Melia, F., & Falcke, H. 2001, ARA&A, 39, 309
Misner, C. W., Thorne, K. S., & Wheeler, J. A. 1973, Gravitation, W. H. Freeman and Co., San Francisco
Morris, M. 1993, ApJ, 408, 496
Paumard, T., et al. 2006, ApJ, 643, 1011
Perets, H. B., Hopman, C., & Alexander, T. 2007, ApJ, 656, 709
Polnarev, S. & Rees, M. J. 1994, A&A, 283, 301
Quinlan, G. D. 1996, NewA, 1, 35
Rauch, K., & Tremaine, S. 1996, New Astronomy, 1, 149
Sanders, R. H. 1992, Nature, 359, 131
Schödel, R., et al. 2002, Nature, 419, 694
Yu, Q., 2002, MNRAS, 331, 935
Yu, Q., & Tremaine, S. 2001, AJ, 121, 1736
Yu, Q., & Tremaine, S. 2003, ApJ, 599, 1129